THE JOURNAL OF PHYSICAL CHEMISTRY B

ARTICLE

pubs.acs.org/JPCB

Hydrodynamic Properties of Magnetic Nanoparticles with Tunable Shape Anisotropy: Prediction and Experimental Verification

Ilya Martchenko,[†,§] Hervé Dietsch,[*,†] Christian Moitzi,[‡] and Peter Schurtenberger[*,§]

[†]Adolphe Merkle Institute and Fribourg Center for Nanomaterials, Route de l'Ancienne Papeterie, CP 209, 1723 Marly 1, Switzerland

[‡]Anton Paar GmbH, Anton Paar Straße 20, 8054 Graz, Austria

[§]Division of Physical Chemistry, Department of Chemistry, Lund University, Box 124, 22100 Lund, Sweden

ABSTRACT:

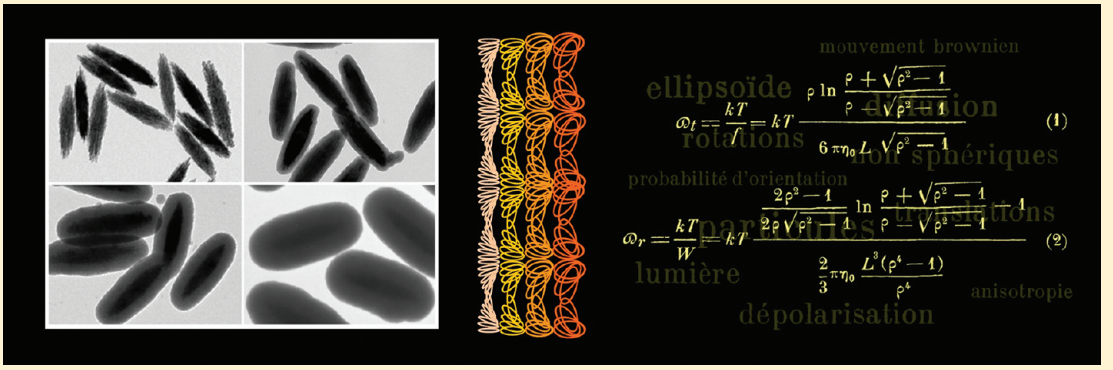

We describe the characterization of the hydrodynamic properties of anisotropic magnetic nanoparticles using a combination of transmission electron microscopy (TEM) and dynamic as well as depolarized dynamic light scattering (DLS/DDLS). The particles used are nearly monodisperse hematite spindles with an average length of 280 nm and a minor axis of 57 nm, coated with a layer of silica of variable thickness that allows us to tune the particle aspect ratio between 5 and 2. Their geometrical dimensions can thus be determined easily and quantitatively from TEM. Moreover, their size is ideal to employ DLS and DDLS to measure the translational and rotational diffusion coefficients D_T and D_R, while the presence of a magnetic core opens a plethora of opportunities for future studies and applications. We demonstrate that we can successfully predict the hydrodynamic properties of the different particles based on a TEM characterization of their size distribution and using established theoretical models for the hydrodynamic properties of anisotropic particles. When compared with the theoretical predictions, our light scattering measurements are in quantitative agreement. This agreement between theory and experiment is achieved without having to invoke any adjustable free parameter, as the TEM results are used to calculate the corresponding diffusion coefficients on an absolute scale. We demonstrate that this is achieved due to a new and simple method for the statistical weighting of the TEM information, and the use of the correct hydrodynamic models for the observed particle shape. In addition, we also demonstrate an enhanced sensitivity of the rotational diffusion for the surface properties of ellipsoidal nanoparticles, and point out that this may serve as an ideal tool toward characterizing functionalized surfaces.

INTRODUCTION

Colloidal particles have frequently been used as versatile model systems to investigate classical problems in condensed matter physics such as nucleation, crystallization, or glass transition. They were successfully employed as models for atomic fluids and solids,[1−3] since size and interactions can be controlled.

The structural properties and the mobility of spherical particles have been extensively investigated in both dilute and concentrated suspensions. Particular emphasis has been given to the investigation of the phenomenon of dynamic arrest, i.e., the occurrence of a glass transition at high particle volume fractions that has been observed for a variety of different interaction potentials.

Over the past decade, the research emphasis has shifted to anisotropic particles or particles interacting via noncentrosymmetric interaction potentials.[4] Morphology, internal structure, composition, shape anisometry, and particle interactions of such colloids may be tuned.[4−7]

A recent example of core−shell particles suitable to be used as a well-defined model system to study structural and dynamic properties of elongated particles is hematite spindles coated with a silica layer. These particles combine well-defined morphologies

Received: August 15, 2011
Revised: September 30, 2011
Published: October 10, 2011

of the core and the shell and are ideal candidates for such studies due to their low polydispersity. The size and aspect ratio of these core−shell particles can be controlled by varying the thickness of the silica coating.[8−11] Sacanna et al.[9] successfully applied similar systems for studying their rotational mobility with rotational fluorescence recovery after photobleaching. We have already previously demonstrated that we can quantitatively describe the structural properties of the individual particles in suspensions using a combination of small-angle X-ray scattering (SAXS) and a theoretical model that incorporates the size distribution and the particle morphology (core and shell) determined by TEM.[12] Moreover, we have also fully characterized their magnetic properties in suspension, and derived a quantitative model in order to describe the effect of external magnetic field on the orientation of these magnetic ellipsoids in dilute suspensions.[12,13]

In a next step, we now look at the dynamical properties of these model particles as a function of the tunable aspect ratio in dilute suspensions, and compare their translational and rotational motion with theoretical predictions based on well established hydrodynamic models for anisotropic particles combined with direct measurements of the size distributions using TEM. This will then set the stage to explore the evolution of the dynamic and static properties of the suspensions at higher volume fractions.

In spheres and certain types of nanorods, polydispersity is reflected only in one linear dimension or degree of freedom. Comparison between measurements and theory for such systems has shown good agreement.[14−18] In contrast, open questions remain on the possibility to directly compare simple theoretical calculations with experimental values for translational and rotational[19] self-mobility of elongated "ellipsoids". Such particles may be polydisperse in length and in aspect ratio, and the 3D curvature may vary from particle to particle. Previously, a discrepancy between theoretical calculation and experiment, sometimes of orders of magnitude, was observed in stretched polystyrene latex[20] and hematite particles.[21]

Experimental tests for the rotational diffusion of anisometric particles are relatively rare,[18,22−26] although appropriate particle systems and instrumentation have become available in recent decades, and theories for elongated particles pioneered by Perrin even in the 1930s.[27,28]

EXPERIMENTAL SECTION

Materials and Methods. *Chemicals.* Tetraethyl orthosilicate (TEOS) (purity >99%) and absolute ethanol were supplied by Merck. Iron III perchlorate $Fe(ClO_4)_3 \cdot 6H_2O$, $NaH_2PO_4 \cdot H_2O$ (purity >98%), tetramethylammonium hydroxide (TMAH) in 25% water solution, poly(vinylpyrrolidone) (PVP) with a molecular weight of 10000 g/mol, and urea (purity >99%) were purchased from Sigma-Aldrich. Deionized water purified with a Milli-Q system (resistivity of 18.2 MΩ · cm) was used exclusively.

Transmission Electron Microscopy (TEM.). A TEM-CM100 microscope from Philips operating at 80 keV was used. Samples were prepared by drying a droplet of a particle dispersion at about 1 wt % onto a carbon coated (300 mesh) grid. Size distributions were determined manually with the aid of UTHSCSA Image-Tool software, from populations of 100−200 particles.

Dynamic Light Scattering (DLS.). Translational diffusion coefficients, D_T, were determined by DLS using a Goniometer System from LS Instruments (Switzerland) equipped with a 632.8 nm He−Ne laser with a maximum power of 20 mW. Dilute suspensions of ∼0.01 wt % were filled into 10 mm cylindrical glass cells and placed in the temperature controlled index matching bath. The scattered light was detected within an angular range of 16−148° by one or two avalanche photodiodes and processed by Flex correlators in autocorrelation and cross-correlation configurations. Translational diffusion coefficients D_T were determined from a cumulant analysis of the correlation functions.

Depolarized Dynamic Light Scattering (DDLS.). A dilute colloidal suspension of ∼0.01 wt % was used for the determination of both rotational D_R and translational D_T diffusion coefficients, in the same Goniometer System from LS Instruments. A polarizing grade calcite prism PGT 2.08 from Bernhard Halle Nachfl. with an extinction ratio better than 10^{-5} was mounted between the sample and detector and aligned perpendicular to the polarization of the incident light (VH geometry). VH geometry was achieved by minimizing the detected scattering intensity of an isotropic sample containing spherical particles, prior to experiments at each angle. VH depolarized dynamic light scattering experiments were determined in the range of 16−148°. Rotational and translational diffusion coefficients were determined via a cumulant analysis of the correlation functions at each scattering angle.

Synthesis of the Particles. *Hematite Cores.* Nanosized spindle-type cores used as templates for the core−shell particles were synthesized following the method originally developed by Ocaña et al.[29] In the synthesis, 199 mmol (92.43 g) of $Fe(ClO_4)_3 \cdot 6H_2O$, 9.4 mmol (1.30 g) of $NaH_2PO_4 \cdot H_2O$, and 200 mmol of urea (12.01 g) were dissolved in 2 L of Milli-Q water in a glass bottle with a tight cap, and placed in a preheated temperature-controlled oven at 98 °C for 24 h. The resulting dispersion was then purified via 10 consecutive centrifugation and redispersion steps, at 10000 rpm for 10 min each. The final hematite stock solution consisted of 5.98 wt % hematite particles in deionized water and was labeled "HS0". All batches of particles have been labeled HS (hematite−silica) followed by an index representing the average thickness of the silica coating in nanometers.

Silica Shells. Hematite spindles were coated with silica layers based on the approach of Graf et al. using poly(vinylpyrrolidone) (PVP) as a stabilizer.[30] This method allowed the concentration of core−shell particles formed to be increased by a factor of 6 compared with the original coating method using an ultrasonic bath.[31] Batches with three different silica thicknesses were synthesized.

Silica coatings were obtained by diluting 4.09 mmol (0.653 g) of hematite dispersed in water from the stock solution HS0 (10.91 g of stock solution) in 230 g of Milli-Q water and adding 1.59 mmol (15.9 g) of PVP with a molecular weight of 10000 g/mol. The system was dispersed with an ultrasonicator for 10 min and then mechanically stirred overnight at 300 rpm. Particles were then centrifuged at 10000 rpm for 10 min, and redispersed in 30 mL of water. They were introduced into a solvent mixture of 109 g of water and 1050 g of ethanol before 1.59 mmol of TMAH (0.58 g of TMAH in 6 g of ethanol) was added dropwise under constant mechanical stirring at 300 rpm. A total of 26.16 mmol of TEOS (5.45 g diluted by 4 mL of ethanol) was added to the reaction mixture in three aliquots, after 30, 50, and 70 min after the addition of TMAH, respectfully. Ultrasonic agitation continued for an hour after the last addition of TEOS. Then, the system was mechanically stirred for 24 h. The coated particles were then centrifuged three times (10000 rpm; 10 min) and

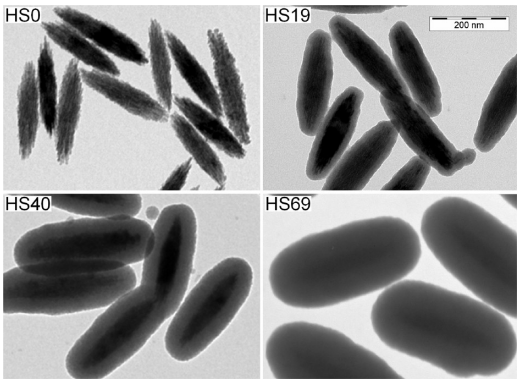

Figure 1. TEM micrographs of uncoated hematite spindles HS0 and silica-coated hematite spindles with one (HS19), two (HS40), and three (HS69) consecutive coatings. Indexes correspond to the average thickness of the silica layers in nanometers. The scale bar, shown for HS19, is valid for all micrographs.

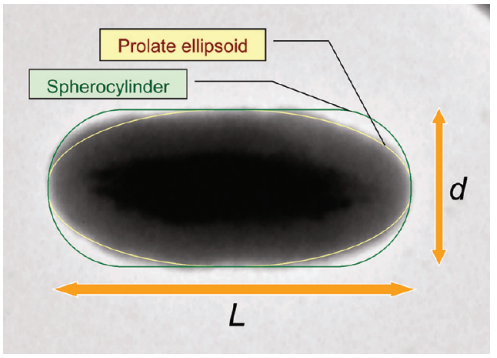

Figure 2. The length L and width d of every particle were determined from coronal sections of particles seen on TEM micrographs. Ellipsoidal and spherocylindrical shapes, reconstructed on the basis of L and d, were observed to be reasonable approximations to the actual particle shape.

redispersed in water, resulting in a stock solution of "HS19" with a concentration of 2.4% wt.

Thicker coatings were achieved by repeating the silica coating process to already coated particles.

"HS40" particles were prepared from 13.44 g of the stock dispersion of HS19 (effective 2.03 mmol of α-Fe_2O_3) with 0.785 mmol (7.85 g) of PVP, 0.79 mmol of TMAH (0.286 g of 25% solution), and effective 12.92 mmol (2.69 g) of TEOS using the same silica coating process.

"HS69" particles were prepared from 13.93 g of a 3.4 wt % dispersion of HS40 (effective 2.96 mmol of α-Fe_2O_3) with 1.15 mmol (11.5 g) of PVP, 1.15 mmol of TMAH (0.42 g of 25% solution), and effective 18.96 mmol (3.95 g) of TEOS using the same procedure.

RESULTS AND DISCUSSION

Structural Properties from TEM. The transmission electron microscopy (TEM) micrographs in Figure 1 show the evolution of the particle morphology with increasing thickness of the porous silica layer.

The TEM data were used to determine the geometrical dimensions (length L and width d.) These two parameters were then used in combination with the geometrical models of either a

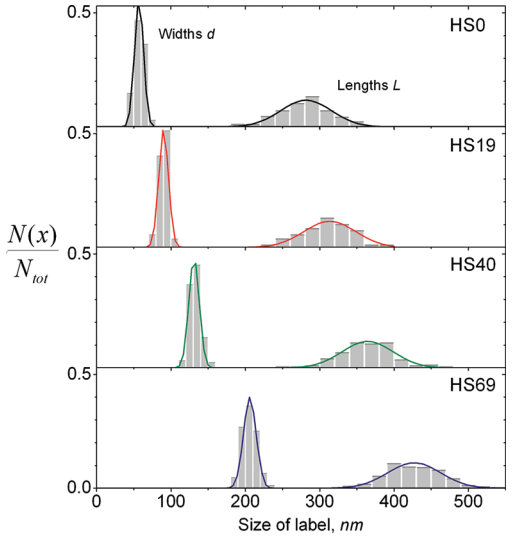

Figure 3. Normalized size distributions of hematite spindles (HS0) and silica-coated hematite spindles HS19, HS40, and HS69, with Gaussian fits. The histogram steps were 20 nm for the length L and 10 nm for the width d.

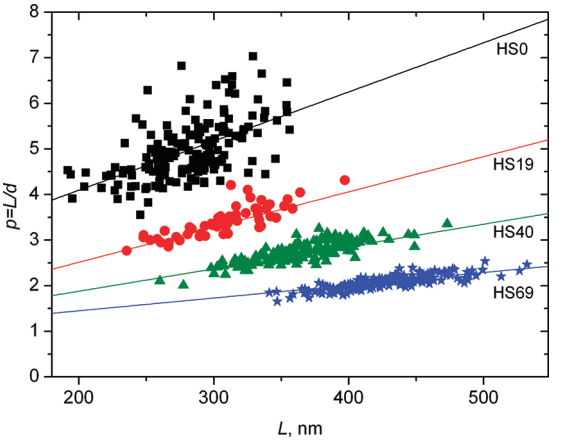

Figure 4. Aspect ratios for every single particle as a function of particle length, for the hematite spindles HS0 (plotted as squares), and silica-coated hematite particles HS19 (circles), HS40 (triangles), and HS69 (stars).

prolate ellipsoid or spherocylinder to completely model the shape of the particles, as illustrated in Figure 2.

The resulting distributions for L and d are shown in Figure 3 for all four model systems.

Figure 4 depicts the distribution of aspect ratios L/d of individual particles from each batch as a function of their length. There is a relationship between L and L/d for each batch, where the slope seems to decrease with increasing shell thickness. At the largest shell thickness, the resulting particles have an almost constant aspect ratio, showing a weak dependence on L only. The trend lines in the figure show that the longer particles in the same batch have larger values of L/d than shorter particles, but this tendency is gradually fading for batches with thicker silica layers. The cumulative result of each silica layer is a reduced influence of core anisometry on the particle anisometry, with particles gradually approaching spherical shapes. The spread in the ordinate illustrates the length polydispersity of the particles.

dx.doi.org/10.1021/jp2078264 |J. Phys. Chem. B 2011, 115, 14838–14845

Table 1. Geometrical Parameters of Hematite Spindles HS0 and Silica-Coated Hematite Particles HS19, HS40, and HS69

	uncoated hematite core (HS0)	core with single silica coating (HS19)	core with double silica coating (HS40)	core with triple silica coating (HS69)
length L, nm	280 ± 35[a]	309 ± 34[a]	361 ± 45[a]	427 ± 36[a]
width d, nm	57 ± 7[a]	90 ± 6[a]	131 ± 13[a]	206 ± 10[a]
$\langle p\rangle = \langle L/d\rangle$	4.97 ± 0.64[a]	3.43 ± 0.35[a]	2.78 ± 0.49[a]	2.07 ± 0.15[a]
$\langle L\rangle/\langle d\rangle$	4.9 ± 1.2[b]	3.4 ± 0.6[b]	2.76 ± 0.62[b]	2.07 ± 0.27[b]
silica thickness, nm		19.2 ± 3.3	40.3 ± 3.8	68.8 ± 4.3
mean volume of the core, nm^3	4.8 × 10^5	4.8 × 10^5	4.8 × 10^5	4.8 × 10^5
mean volume of the silica coating, nm^3		8.4 × 10^{5c}	27.7 × 10^{5c}	90.1 × 10^{5c}
mean volume of the entire particle, nm^3	4.8 × 10^{5c}	13.2 × 10^{5c}	32.5 × 10^{5c}	94.9 × 10^{5c}

[a] Statistical standard deviation within the data set. [b] Error was calculated through standard deviations of $\langle L\rangle$ and $\langle d\rangle$. [c] Calculated via population means for linear sizes of uncoated cores HS0 and coated particles, with cores and particles as a whole modeled by prolate ellipsoids and shells modeled by a layer limited by two prolate ellipsoids.

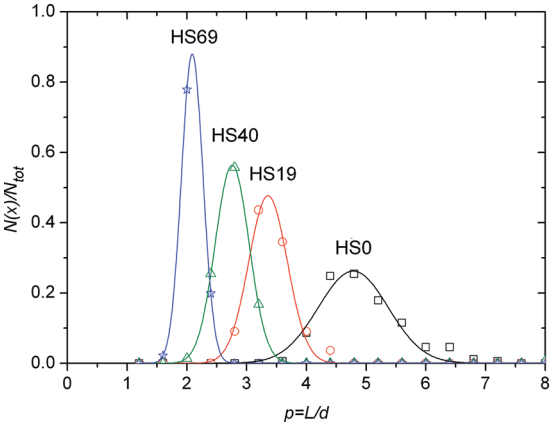

Figure 5. Distribution of aspect ratios for the particles HS0 (plotted as squares), HS19 (circles), HS40 (triangles), and HS69 (stars).

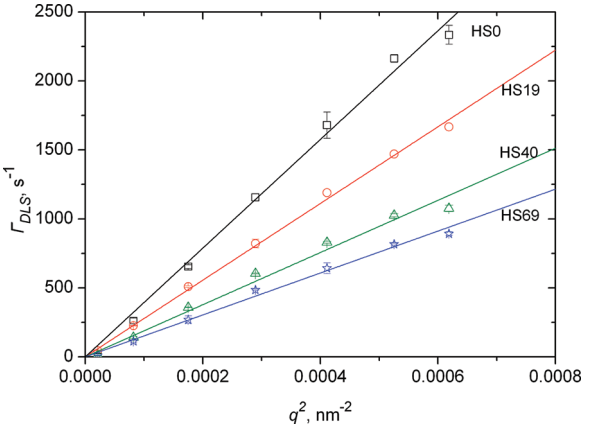

Figure 6. Decay rates Γ_{DLS} of polarized dynamic light scattering, plotted as a function of squared scattering vector q^2, for the particles HS0 (plotted as squares), HS19 (circles), HS40 (triangles), and HS69 (stars).

Table 1 summarizes all the important measured and calculated parameters describing the morphology of four batches. Figure 5 illustrates the distribution of aspect ratios for the studied batches, and indicates that the aspect ratios follow a normal distribution. Furthermore, the data in Table 1 shows that the mean aspect ratio is close to the ratio between the mean length and the mean width.

Translational and Rotational Diffusion. Translational and rotational diffusion coefficients were determined via light scattering techniques. In polarized dynamic light scattering (DLS), the decay rate Γ_{DLS} of the correlation function provides the translational diffusion coefficient through

$$\Gamma_{DLS} = q^2 D_T \quad (1)$$

with the magnitude of the scattering vector q given by $q = (4\pi n/\lambda_0)\sin(\theta/2)$, where θ is the scattering angle, n is the solvent refractive index, and λ_0 is the wavelength of the incident beam in vacuum.

The decay rate Γ_{DDLS} of correlation functions in depolarized light scattering studies (DDLS) is related to the translational (D_T) and rotational (D_R) diffusion coefficients via

$$\Gamma_{DDLS} = q^2 D_T + 6D_R \quad (2)$$

Figure 6 shows the plotted decay rates Γ_{DLS} as a function of q^2. Γ_{DLS} increases linearly with q^2, in good agreement with eq 1. The slopes of linear fits (eq 1) give the translational diffusion coefficients D_T.

Figure 7 shows the corresponding dependence for the depolarized decay rates Γ_{DDLS}. While the slopes still yield the translational diffusion coefficients D_T (eq 2), the intercepts of the fits contain the information on the rotational diffusion coefficient D_R (eq 2).

The experimental values for D_T and D_R are shown in Tables 2 and 3, respectively. Translational diffusion coefficients determined with both methods differ only slightly from each other (Table 2).

Diffusion coefficients were theoretically calculated from statistical TEM data and compared with the experimental values. Two simple models have been tested, the Perrin theory for ellipsoids (with the retrospective corrections made by Koenig)[27,28,32] and the theories for spherocylindrical particles, developed by Norisuye et al.[33] and Yoshizaki et al.[34] Both models look promising, as they are analytical, do not require time-consuming numerical simulation, and allow describing the dynamics of nanoscale systems of different nature.[14,35−37] The final expressions, given in the Appendix, were algebraically simplified and transformed to a form where length L and aspect ratio $p = L/d$ are the two free parameters which determine the particle shape.

Below, we will now quantitatively compare the predictions from both models with the experimentally determined diffusion coefficients.

The relationship between the diffusion coefficients (translational D_T; rotational D_R) and friction factors or drag coefficients (translational f, rotational W) for both translational and rotational diffusion is given by the Einstein relations:

$$D_T = \frac{k_B T}{f} \tag{3}$$

$$D_R = \frac{k_B T}{W} \tag{4}$$

where k_B is the Bolzmann constant, T the absolute temperature, f the translational friction, and W the rotational friction coefficient for a particle.

In order to directly compare the measured diffusion coefficients with TEM-based theoretical predictions, proper weighting across the monomodal population of particles is necessary. Larger particles contribute more to light scattering, as the scattered intensity is proportional to the square of the volume of a single particle. The corresponding weighting across less than 100−200 particles from each of the four batches was made via

$$\langle D \rangle = \frac{\sum_i D_i V_i^2}{\sum_i V_i^2} \tag{5}$$

where D_i and V_i are the diffusion coefficients (rotational or translational) and the volume of each particle in the batch, respectively. To perform this weighting, volumes according to each of the models were reconstructed via 2D linear dimensions derived from TEM images of coronal sections of particles.

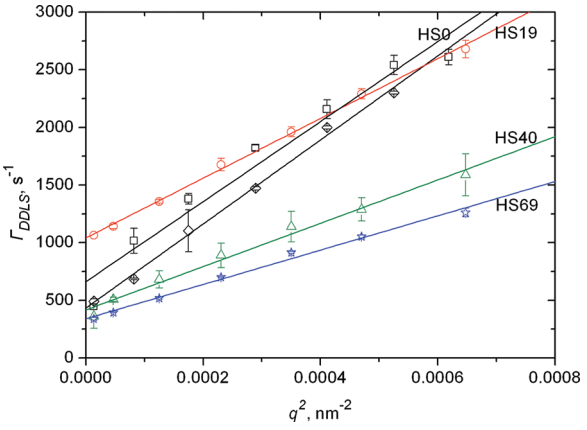

Figure 7. Decay rates Γ_{DDLS} of depolarized dynamic light scattering, plotted as a function of squared scattering vector q^2, for the particles HS0 measured at pH 7 (plotted as squares) and pH 10 (diamonds), HS19 (circles), HS40 (triangles), and HS69 (stars).

A comparison between the data for the translational diffusion coefficients calculated for the four batches of particles and the results of the measurements performed by DLS and DDLS are shown in Table 2.

A more direct and visual comparison between the TEM-based prediction and the experimental values of D_T can be made by plotting the theoretical values of D_T versus particle length L but requires taking into account the dependence of the aspect ratio p on length L. The dependence of the average aspect ratio $\langle p \rangle$ on the average length $\langle L \rangle$ was fitted with a hyperbola. The resulting diffusion coefficients are plotted against particle length in Figure 8 (solid lines). The dotted lines in Figure 8 correspond to confidence intervals for D_T in each model, calculated from the maximum $(\langle p \rangle + \sigma)$ and minimum values $(\langle p \rangle - \sigma)$ of aspect ratios p with distribution standard deviation σ for every batch, and similarly interpolated with a hyperbola.

Both models quantitatively match with the experimental data, with the spherocylindrical model possibly providing slightly better results.

A significantly slower dynamics for uncoated hematite spindles HS0 has been observed during measurements performed prior to vigorous ultrasonic agitation, not shown here, indicating some aggregation of the uncoated hematite particles. This observation is in agreement with previous studies of aggregation and stability of hematite ellipsoids in aqueous suspensions,[38] and probably

Table 2. TEM-Based Theoretical Expectations and Measured DLS and DDLS Data on Translational Mobility of Particles

batch	Perrin model, f_p, Js/m^2	Perrin model, weighted $\langle D_T \rangle_p$, m^2/s	spherocylinder model, f_{sp}, Js/m^2	spherocylinder model, weighted $\langle D_T \rangle_{sp}$, m^2/s	D_T (DLS), m^2/s	D_T (DDLS), m^2/s
HS0	$(1.14 \pm 0.11) \times 10^{-9}$	3.405×10^{-12}	$(1.25 \pm 0.12) \times 10^{-9}$	3.101×10^{-12}	$(3.93 \pm 0.08) \times 10^{-12}$	$(3.47 \pm 0.32) \times 10^{-12}$ $(3.65 \pm 0.12) \times 10^{-12}$ [a]
HS19	$(1.46 \pm 0.11) \times 10^{-9}$	2.702×10^{-12}	$(1.61 \pm 0.12) \times 10^{-9}$	2.461×10^{-12}	$(2.78 \pm 0.04) \times 10^{-12}$	$(2.59 \pm 0.06) \times 10^{-12}$
HS40	$(1.91 \pm 0.19) \times 10^{-9}$	2.066×10^{-12}	$(2.09 \pm 0.21) \times 10^{-9}$	1.888×10^{-12}	$(1.89 \pm 0.06) \times 10^{-12}$	$(1.88 \pm 0.10) \times 10^{-12}$
HS69	$(2.59 \pm 0.15) \times 10^{-9}$	1.564×10^{-12}	$(2.80 \pm 0.16) \times 10^{-9}$	1.420×10^{-12}	$(1.52 \pm 0.03) \times 10^{-12}$	$(1.49 \pm 0.06) \times 10^{-12}$

[a] Repeated measurement at pH 10.

Table 3. TEM-Based Theoretical Expectations and Measured DDLS Data on Rotational Mobility of Particles[a]

batch	Perrin model, W_p, kgm^2/s	Perrin model, weighted $\langle D_R \rangle_p$, s^{-1}	spherocylinder model, W_{sp}, kgm^2/s	spherocylinder model, weighted $\langle D_R \rangle_{sp}$, s^{-1}	D_R (DDLS), s^{-1}
HS0	$(1.35 \pm 0.42) \times 10^{-23}$	284	$(1.78 \pm 0.55) \times 10^{-23}$	216	110 ± 20 72 ± 6 [a]
HS19	$(2.24 \pm 0.60) \times 10^{-23}$	177	$(2.87 \pm 0.79) \times 10^{-23}$	138	174 ± 3
HS40	$(4.34 \pm 1.05) \times 10^{-23}$	90.7	$(5.43 \pm 1.36) \times 10^{-23}$	72.4	70 ± 6
HS69	$(8.92 \pm 1.78) \times 10^{-23}$	46.6	$(10.73 \pm 2.23) \times 10^{-23}$	36.9	57 ± 4

[a] Repeated measurement at pH 10.

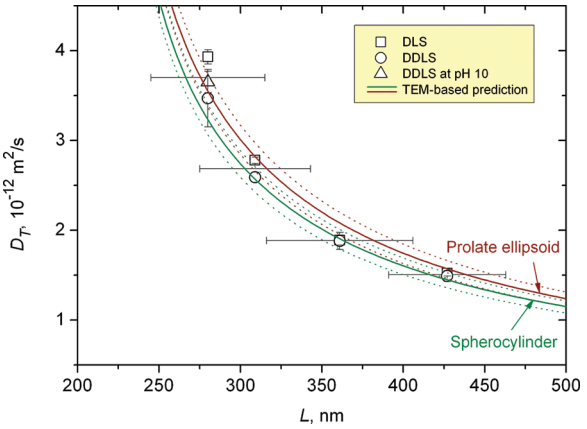

Figure 8. Translational diffusion coefficients measured with DLS (plotted as squares) and DDLS (circles) compared with theoretical curves as a function of particle length. Dotted curves correspond to deviations caused by standard deviation σ for aspect ratios. Horizontal bars correspond to the length polydispersity of the particles. An extra data point measured with DDLS at pH 10 for the particles HS0, plotted as a triangle, was performed to exclude aggregation for this batch.

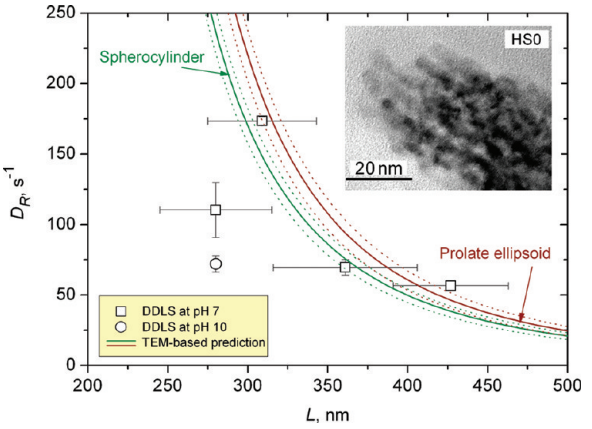

Figure 9. Rotational diffusion coefficients measured with DDLS were compared with theoretical curves as a function of the length of particles. Dotted curves correspond to deviations caused by a standard deviation σ for the aspect ratios. Horizontal bars correspond to the length polydispersity of the particles. The reference data for the hematite spindles HS0 at pH 10 is plotted as a circle. A retarded rotational mobility of the particles HS0 is considered to be linked to high porosity of the hematite particles, clearly seen on a high-resolution TEM micrograph in the inset (see ref 13 for more details).

reflects the fact that the isoelectric point of hematite particles is close to pH 8, whereas the silica coating shifts it to pH 4, i.e., enhancing the stability at neutral pH.[39]

Figure 8 suggests that, despite the porosity of the silica layer and the hematite core,[12,13] the particles in suspension undergo translational diffusion as nondraining smooth hydrodynamic bodies with linear dimensions equal to those determined from independent TEM micrographs.

In a next step, we can also analyze the data for the rotational diffusion. The corresponding values for the rotational diffusion calculated for the four batches of particles and a comparison with the data obtained from depolarized DLS are shown in Table 3.

Figure 9 illustrates the comparison between TEM-based theoretical predictions for rotational diffusion coefficient D_R and DDLS measurements. The results of Figure 9 suggest that both models describe well the rotational behavior of silica-coated particles, with a marked exception for the uncoated hematite spindles HS0, where the measured rotational diffusion is significantly slower than theoretical expectations.

To rule out aggregation as the cause of this discrepancy, independent measurements were repeated at neutral pH and at pH 10, where the surface charge density of the uncoated hematite particles and thus their stability is enhanced. These additional measurements (see Figure 9) clearly showed the reproducibility of the effect. Indeed, the retarded rotational relaxation of HS0 cannot be linked to aggregation, as the *same* DDLS measurements fully agree with the values of D_T predicted for individual, randomly oriented particles (Figure 8).

In order to rule out possible systematic errors in our experimental approach as the source of the discrepancy between prediction and experimental data for the sample HS0, a further test was performed using a different technique and a different solvent. All four batches were dispersed in glycerol, and the values of D_R were determined via the flow dichroism technique, namely, measuring relaxation of the dichroism upon cessation of flow in a Couette geometry.[26,40] While these rheo-optical studies will be reported in a separate manuscript, they quantitatively reproduced the slow rotational relaxation of D_R of HS0 found with DDLS.

Currently, we can thus only speculate about the origin of this marked discrepancy between the theoretical prediction and the measured values of D_R for the uncoated hematite spindles. We believe that this is linked to the very high porosity of the hematite spindles used, as revealed by the high resolution TEM picture shown in the inset of Figure 9, already reported in a previous publication.[13] It appears as if the resulting high surface roughness mostly affects the rotational motion of the particles, while the translational motion that is dominated by diffusion along the long axis seems much less influenced. For the coated particles, the high porosity of the hematite core is then effectively reduced by the silica layer with its much lower porosity.

CONCLUSIONS

Silica-coated hematite particles are ideal model systems to look at hydrodynamic properties of anisotropic colloids. The particles are nearly monodisperse, with aspect ratios tunable between 2 and 5, and geometrical dimensions that can be easily determined independently from TEM. Moreover, their size is ideal to employ DLS and DDLS to determine D_T and D_R.

The TEM-based size distributions have been used together with two well-established theoretical models (ellipsoids and spherocylinders) to predict D_T and D_R without any adjustable parameters. These calculations are based on a newly proposed simple method that relies on the statistical weighting of information derived from TEM, where thus only a limited number of counts are necessary. Our results show very good quantitative agreement between theoretical predictions and experimental findings. For the given particle dimensions, the predictions from both models do agree within experimental accuracy. The relative deviation between prediction and measurement typically corresponds to less than ca. 10−20 nm in particle dimensions, i.e., ca. 5% of the absolute particle length. This is comparable with the errors of the length measurements on TEM micrographs, and lower than the distribution standard deviations for values of L reported in Table 1.

We thus reach significantly different conclusions with respect to the accuracy of the applied experimental techniques (TEM and DDLS/DLS) than published recently by Reddy et al.[26] We believe that this is due to the fact that the number of TEM counts needed to achieve the necessary precision of the statistical averages was estimated incorrectly in ref 26. Moreover, the discrepancies between the two techniques reported in ref 26 can be explained and removed if more appropriate mathematical model (spherocylindrical, not cylindrical) and data treatment routines are used for analyzing the raw DDLS data.

We believe that our results clearly demonstrate that a combination of DLS, DDLS, and TEM is ideally suited to obtain quantitative information on the size, shape, and dimensions for anisotropic nanoparticles.

A single but marked exception from this trend is found for the D_R of uncoated hematite spindles HS0, probably related to the high porosity of the particles. This indicates a much higher sensitivity of the rotational diffusion to surface properties of the particles, in comparison to the translational diffusion, which could provide important information when analyzing surface properties of anisotropic nanoparticles in the future. However, it is clear that this feature requires additional theoretical and experimental input.

On the basis of our results, we are now in a good position to tackle the influence of interparticle interaction on particle mobility, and investigate the evolution of the structural and dynamic properties of anisotropic particle suspensions, at higher concentrations.

APPENDIX

The translational friction coefficient f_p for a single prolate ellipsoidal particle with a random orientation (statistically averaged over all angles) is derived[27] from the friction coefficients for ellipsoids along their long and short axes.[41,42] We bring the expression to the shortest form:

$$f_p = \frac{3\pi\eta_0 L\sqrt{p^2-1}}{p\ln(p+\sqrt{p^2-1})} \tag{6}$$

where L is the length of the particle, η_0 is the solvent viscosity, and $p = L/d$ is the aspect ratio ($p > 1$) of a particle with length L and diameter d.

The translational friction coefficient f_{sp} for a single spherocylindrical particle[33] with a random orientation may be expressed as[43]

$$f_{sp} = \frac{3\pi\eta_0 L}{\ln p + \sum_{i=0}^{5} a_i p^{-i}} \tag{7}$$

where a_i are as follows: $a_0 = 0.3863$, $a_1 = 0.6863$, $a_2 = -0.06250$, $a_3 = -0.01042$, $a_4 = -0.000651$, and $a_5 = 0.0005859$.

The rotational friction coefficient W_p for a single prolate ellipsoidal particle rotating about the short equatorial axes[28,32] may be brought to the shortest form:

$$W_p = \frac{\frac{2}{3}\pi\eta_0 L^3\frac{p^4-1}{p^4}}{\frac{(2p^2-1)\ln(p+\sqrt{p^2-1})}{p\sqrt{p^2-1}} - 1} \tag{8}$$

Note that despite a known[32] error in Perrin's original algebra, there have been some recent cases of confusion in the literature with regard to this analytical expression (a wrong sign under the root in the term $\ln(p + (p^2 - 1)^{1/2})$,[44] or misattribution of prolate and oblate dynamics[45]).

The rotational friction coefficient W_{sp} for a single spherocylindrical particle rotating about the short equatorial axes[34,43] can be expressed as

$$W_{sp} = \frac{\pi\eta_0 L^3}{3\left(\ln p + 2\ln 2 - \frac{11}{6} + \frac{\ln 2}{\ln(1+p)}\left(\frac{1}{3} - 2\ln 2 + \frac{11}{6} - \sum_{i=1}^{6} a_i\right) + \sum_{i=1}^{6} a_i p^{-i/4}\right)} \tag{9}$$

where a_i are as follows: $a_1 = 13.04468$, $a_2 = -62.6084$, $a_3 = 174.0921$, $a_4 = -218.8365$, $a_5 = 140.26992$, $a_6 = -33.27076$.

AUTHOR INFORMATION

Corresponding Author

*E-mail: herve.dietsch@unifr.ch (H.D.); peter.schurtenberger@fkem1.lu.se (P.S.).

ACKNOWLEDGMENT

We thank Otto Glatter and Jérôme J. Crassous for important advice concerning the DDLS technique and the data treatment. We extend our gratitude to Naveen Krishna Reddy and Jan Vermant for their expert help in corroborating some of the conclusions via flow dichroism tests, and to Bernard Grobéty and Mathias Reufer for a high-resolution TEM image. We acknowledge equally Olivier Pravaz, Vikash Malik, and Benoît Droz for assistance with TEM, and appreciate the helpful discussions with Verena Städele and Graeme Gillies. Financial support from the Adolphe Merkle Foundation, the Swiss National Science Foundation, COST action D43, the Swiss State Secretariat for Education and Research, and the SoftComp network is gratefully acknowledged.

REFERENCES

(1) Pusey, P. N.; van Megen, W. Phase behaviour of concentrated suspensions of nearly hard colloidal spheres. *Nature* **1986**, *320*, 340–342.

(2) Anderson, V. J.; Lekkerkerker, H. N. W. Insights into phase transition kinetics from colloid science. *Nature* **2002**, *416*, 811–815.

(3) Poon, W. Colloids as big atoms. *Science* **2004**, *304* (5672), 830–831.

(4) Glotzer, S. C.; Solomon, M. J. Anisotropy of building blocks and their assembly into complex structures. *Nat. Mater.* **2007**, *6*, 557–562.

(5) Dietsch, H.; Malik, V.; Reufer, M.; Dagallier, C.; Shalkevich, A.; Sarić, M.; Gibaud, T.; Cardinaux, F.; Scheffold, F.; Stradner, A.; Schurtenberger, P. Soft nanotechnology - from colloid physics to nanostructured functional materials. *Chimia* **2008**, *62*, 805–814.

(6) Sacanna, S.; Rossi, L.; Wouterse, A.; Philipse, A. P. Observation of a shape-dependent density maximum in random packings and glasses of colloidal silica ellipsoids. *J. Phys.: Condens. Matter* **2007**, *19*, 376108.

(7) van der Kooij, F. M.; Kassapidou, K.; Lekkerkerker, H. N. W. Liquid crystal phase transitions in suspensions of polydisperse plate-like particles. *Nature* **2000**, *406*, 868–871.

(8) Thies-Weesie, D. M. E.; Philipse, A. P.; Kluijtmans, S. G. J. M. Preparation of sterically stabilized silica-hematite ellipsoids: sedimentation, permeation, and packing properties of prolate colloids. *J. Colloid Interface Sci.* **1995**, *174*, 211–223.

(9) Sacanna, S.; Rossi, L.; Kuipers, B. W. M.; Philipse, A. P. Fluorescent monodisperse silica ellipsoids for optical rotational diffusion studies. *Langmuir* **2006**, *22* (4), 1822–1827.

(10) Dietsch, H.; Reufer, M.; Malik, V.; Schurtenberger, P. Magnetic nanoparticles with variable size and shape and surface functionality as switchable building blocks for soft nanotechnology. *NSTI-Nanotech2008* **2008**, *1* (2), 226–229.

(11) Ding, T.; Liua, Zh.; Songa, K.; Tunga, Ch.-H. Synthesis of monodisperse ellipsoids with tunable aspect ratios. *Colloids Surf., A* **2009**, *336* (1−3), 29–34.

(12) Reufer, M.; Dietsch, H.; Gasser, U.; Hirt, A.; Menzel, A.; Schurtenberger, P. Morphology and orientational behavior of silica-coated spindle-type hematite particles in a magnetic field probed by small-angle X-ray scattering. *J. Phys. Chem. B* **2010**, *114* (12), 4763–4769.

(13) Reufer, M.; Dietsch, H.; Gasser, U.; Grobéty, B.; Hirt, A. M.; Malik, V. K.; Schurtenberger, P. Magnetic properties of silica coated spindle-type hematite particles. *J. Phys.: Condens. Matter* **2011**, *23* (6), 065102.

(14) Tirado, M. M.; Martínez, C. L.; García de la Torre, J. Comparison of theories for the translational and rotational diffusion coefficients of rod-like macromolecules. Application to short DNA fragments. *J. Chem. Phys.* **1984**, *81* (4), 2047–2052.

(15) Brogioli, D.; Salerno, D.; Cassina, V.; Sacanna, S.; Philipse, A. P.; Croccolo, F.; Mantegazza, F. Characterisation of anisotropic nanoparticles by using depolarized dynamic light scattering in near field. *Opt. Express* **2009**, *17* (3), 1222–1233.

(16) Piazza, R.; Degiorgio, V. Rotational and translational self-diffusion coefficients of interacting Brownian spheres. *J. Phys.: Condens. Matter* **1993**, *5* (34B), B173–B182.

(17) Koenderink, G. H.; Sacanna, S.; Aarts, D. G. A. L.; Philipse, A. P. Rotational and translational diffusion of fluorocarbon tracer spheres in semidilute xanthan solutions. *Phys. Rev. E* **2004**, *69*, 021804.

(18) Rodríguez-Fernández, J.; Pérez-Juste, J.; Liz-Marzán, L. M.; Lang, P. R. Dynamic light scattering of short Au rods with low aspect ratios. *J. Phys. Chem. C* **2007**, *111* (13), 5020–5025.

(19) Koenderink, G. H.; Zhang, H. Y.; Aarts, D. G. A. L.; Lettinga, M. P.; Philipse, A. P.; Nagele, G. On the validity of Stokes−Einstein−Debye relations for rotational diffusion in colloidal suspensions *Faraday Discuss.* **2003**, *123*, 335–354.

(20) Matsuoka, H.; Morikawa, H.; Yamaoka, H. Rotational diffusion of ellipsoidal latex particles in dispersion as studied by depolarized dynamic light scattering. *Colloids Surf., A* **1996**, *109*, 137–145.

(21) Quirantes, A.; Ben-Taleb, A.; Delgado, A. V. Determination of size/shape parameters of colloidal ellipsoids by photon correlation spectroscopy. *Colloids Surf., A* **1996**, *119* (1), 73–80.

(22) Zero, K. M.; Pecora, R. Rotational and translational diffusion in semidilute solutions of rigid-rod macromolecules. *Macromolecules* **1982**, *15* (1), 87–93.

(23) Lehner, D.; Lindner, H.; Glatter, O. Determination of the translational and rotational diffusion coefficients of rodlike particles using depolarized dynamic light scattering. *Langmuir* **2000**, *16* (4), 1689–1695.

(24) Hoffmann, M.; Wagner, C. S.; Harnau, L.; Wittemann, A. 3D Brownian diffusion of submicron-sized particle clusters. *ACS Nano* **2009**, *3* (10), 3326–3334.

(25) Shetty, A. M.; Wilkins, G. M. H.; Nanda, J.; Solomon, M. J. Multi-angle depolarized dynamic light scattering of single-walled carbon nanotubes. *J. Phys. Chem. C* **2009**, *113*, 7129–7133.

(26) Reddy, N. K.; Pérez-Juste, J.; Pastoriza-Santos, I.; Lang, P. R.; Dhont, J. K. G.; Liz-Marzán, L. M.; Vermant, J. Flow dichroism as a reliable method to measure the hydrodynamic aspect ratio of gold nanoparticles. *ACS Nano* **2011**, *5* (6), 4935–4944.

(27) Perrin, F. Mouvement brownien d'un ellipsoïde (II). Rotation libre et dépolarisation des fluorescences. Translation et diffusion des molécules ellipsoïdales. *J. Phys. Radium* **1936**, *VII* (1), 1–11.

(28) Perrin, F. Mouvement brownien d'un ellipsoïde (I). Dispersion diélectrique pour des molécules ellipsoïdales. *J. Phys. Radium* **1934**, *V* (10), 497–511.

(29) Ocaña, M.; Morales, M. P.; Serna, C. J. Homogeneous precipitation of uniform alpha-Fe_2O_3 particles from iron salts solutions in the presence of urea. *J. Colloid Interface Sci.* **1999**, *212* (2), 317–323.

(30) Graf, C.; Vossen, D. L. J.; Imhof, A.; van Blaaderen, A. A general method to coat colloidal particles with silica. *Langmuir* **2003**, *19* (17), 6693–6700.

(31) Ohmori, M.; Matijević, E. Preparation and properties of uniform coated colloidal particles. VII. Silica on hematite. *J. Colloid Interface Sci.* **1992**, *150* (2), 594–598.

(32) Koenig, S. H. Brownian motion of an ellipsoid. A correction to Perrin's results. *Biopolymers* **1975**, *14* (11), 2421–2423.

(33) Norisuye, T.; Motowoka, M.; Fujita, H. Wormlike chains near the rod limit: translational friction coefficient. *Macromolecules* **1979**, *12* (2), 320–323.

(34) Yoshizaki, T.; Yamakawa, H. Dynamics of spheroid-cylindrical molecules in dilute solution. *J. Chem. Phys.* **1980**, *72* (1), 57–69.

(35) Löwen, H. Brownian motion of hard spherocyliners. *Phys. Rev. E* **1994**, *50* (2), 1232–1242.

(36) Tsvetkov, N. V.; Andreeva, L. N.; Filippov, S. K.; Bushin, S. V.; Bezrukova, M. A.; Marchenko, I. A.; Strelina, I. A.; Alyab'eva, V. P.; Girbasova, N. V.; Bilibin, A. Yu. Hydrodynamic, optical, and electrooptical properties of macromolecules of third-generation cylindrical dendrimers in chloroform and dichloroacetic acid. *Polym. Sci., Ser. A* **2010**, *52* (1), 8–18.

(37) Martchenko, I.; Tsvetkov, V. Third-generation cylindrical dendrimers based on *L*-aspargic acid in solutions: hydrodynamic and electrooptical properties. *Proc. MIPT* **2010**, *2* (2), 28–34.

(38) Plaza, R. C.; Quirantes, A.; Delgado, A. V. Stability of dispersions of colloidal hematite/yttrium oxide core-shell particles. *J. Colloid Interface Sci.* **2002**, *252* (1), 102–108.

(39) Rufier, C.; Reufer, M.; Dietsch, H.; Schurtenberger, P. A single step hybrid coating process to enhance the electrosteric stabilisation of inorganic particles. *Langmuir* **2011**, *27* (11), 6622–6627.

(40) Vermant, J.; Yang, H.; Fuller, G. G. Rheo-optical determination of aspect ratio and polydispersity of nonspherical particles. *AIChE J.* **2001**, *47*, 790–798.

(41) Gans, R. Zur Theorie der Brownschen Molekularbewegung. *Ann. Phys.* **1928**, *391* (12), 628–656.

(42) Herzog, R. O.; Illig, R; Kudar, H. Über die Diffusion in molekulardispersen Lösungen. *Z. Phys. Chem.* **1933**, *A167* (3), 329–342.

(43) Tsvetkov, V. N. *Rigid-Chain Polymers: Hydrodynamic and Optical Properties in Solution*; Nauka: Leningrad, 1986; Plenum Press: New York, 1989; pp 39, 41.

(44) Lakowicz, J. R. *Principles of Fluorescence Spectroscopy*; Springer Verlag: Berlin, Heidelberg, 2006; p 421.

(45) Loman, A.; Gregor, I.; Stutz, Ch.; Mund, M.; Enderlein, J. Measuring rotational diffusion of macromolecules by fluorescence correlation spectroscopy. *J. Photochem. Photobiol.* **2010**, *9* (5), 627–636.